RESEARCH ARTICLE | JULY 24 2013

Tuning properties of columnar nanocomposite oxides

Zhaoliang Liao; Peng Gao; Shane Stadler; Rongying Jin; Xiaoqing Pan; E. W. Plummer; Jiandi Zhang

Appl. Phys. Lett. 103, 043112 (2013)
https://doi.org/10.1063/1.4816596

Tuning properties of columnar nanocomposite oxides

Zhaoliang Liao,[1] Peng Gao,[2] Shane Stadler,[1] Rongying Jin,[1] Xiaoqing Pan,[2] E. W. Plummer,[1,a)] and Jiandi Zhang[1,a)]
[1]*Department of Physics and Astronomy, Louisiana State University, Baton Rouge, Louisiana 70810, USA*
[2]*Department of Materials Science and Engineering, University of Michigan, Ann Arbor, Michigan 48109, USA*

(Received 29 April 2013; accepted 8 July 2013; published online 24 July 2013)

One major challenge for engineering functional nanocomposites is how to tune the geometry structure and control the chemical composition. We demonstrate here that columnar nanocomposite films can be grown by using alternate deposition of $La_{2/3}Sr_{1/3}MnO_3$ and V_2O_3 on $LaAlO_3$ (111). A solid state reaction, rather than simple spinodal decomposition, dictates the nanocomposite structure, chemical composition, and functionality. By controlling the deposition time ratio of the two compounds, the physical properties of the composite films can be tuned, thus providing a flexible way to tailor nanocomposites for advanced functionality. © *2013 AIP Publishing LLC*. [http://dx.doi.org/10.1063/1.4816596]

Electrons are strongly correlated in many transition-metal oxides (TMOs), giving rise to a remarkable array of exotic properties such as high temperature superconductivity, multiferroicity, and colossal magnetoresistance. These electron correlations induce local entanglement between charge, spin, orbital, and lattice, generating multiple ground states with comparable energy. Hence, a subtle change in local environment can often cause huge and synergetic response in global physical properties. This provides an ideal platform to manipulate physical properties of a system. In past two decades, a variety of experimental and theoretical work have demonstrated their tunability of physical properties with the application of electric or magnetic field, pressure, strain, dimensionality, and chemical doping.[1] The effects are particularly vivid when TMOs are grown in a thin film form. Examples include 2D electron gas and superconductivity at the interface of two insulators,[2,3] enhanced magnetism[4,5] and polarization[6] in planar heteroepitaxial multilayers, unusual multiferroic behavior[7] and enhanced superconducting critical current[8] in columnar nanocomposite epitaxial films. While the origin of these emergent phenomena remains in debate, two schools of thought are vital: one is lattice mismatch,[9] and the other is chemical composition modification[10,11] at the interfaces.

Epitaxial planar multilayers and heterostructures grown layer by layer have been the focus of exploration of interface properties.[2–6,12,13] On the other hand, exploiting vertical heteroepitaxial composite films to create self-assembled nanostructures[14] has also emerged in last few years. It is found that multifunctionality in addition to the enhancement of a single functionality can be realized in nanocomposites.[7,8,14–17] For example, multiferroics can be created by embedding $CoFe_2O_4$ nanocolumns into $BaTiO_3$ matrix.[7] The "colossal" magnetoresistance property of $La_{2/3}Ca_{1/3}MnO_3$ can be controlled by the tensile strain induced by MgO in the immiscible $(La_{2/3}Ca_{1/3}MnO_3)_{1-x}\cdot(MgO)_x$ composite films.[18] However, much of the effort in the community has focused on the control of the structure rather than chemical composition in nanocomposites when designing interface-induced functionality.[14] In this report, we demonstrate a method of tuning functionalities via controlling composite composition by growing columnar nanocomposites of $La_{2/3}Sr_{1/3}MnO_3$-V_2O_3 on $LaAlO_3$ (LAO) (111) substrate. The physical properties of resultant composite films are found to depend solely on the deposition time ratio of two composites.

Traditionally, a nanocomposite film can be obtained via mixed target deposition where two materials are uniformly mixed together in a chemical ratio and pressed into a single target. In this case, the chemical ratio can only be tuned via remaking a target with a different chemical ratio.[7,8,14–17] Another possible approach, which is used in this study, is to grow a nanocomposite film by alternately depositing different oxides (see Fig. 1(a)). In general, a small lattice mismatch between two deposited oxides may lead to a layer by layer planar structure, while a large lattice mismatch will favor the formation of a self-assembled columnar nanocomposite.[7,8,14–17] In this scenario, the chemical ratio as well as geometric structure may be tuned simply by controlling the relative deposition time. In particular, nanocomposite films may be formed by exploiting the lattice mismatch.

We use $La_{2/3}Sr_{1/3}MnO_3$ (LSMO) and V_2O_3 as two target materials and grow composite films on LAO (111) substrates via alternate deposition by using pulsed laser deposition (PLD). LSMO is a well-known ferromagnetic (FM) metal in the ground state exhibiting colossal magnetoresistance.[19] With increasing temperature, the LSMO undergoes a FM metal to paramagnetic (PM) "bad metal" transition at ~370 K while maintaining its rhombohedral lattice structure. On the other hand, V_2O_3 is a Mott-insulator with antiferromagnetic (AFM) insulating ground state and has a transition to PM metal at 160 K on warming, accompanied by a monoclinic to rhombohedral structure transition.[20] Both LSMO and V_2O_3 are rhombohedral at room-temperature, but having ~11% lattice mismatch in the a-b plane and 4% mismatch in c direction. With such large lattice mismatch, the combination of these two compounds is expected to form a nanocomposite.

All the composite films as well as pure LSMO and V_2O_3 thin films were grown in the same growth condition on LAO (111) substrates by a ultra-high vacuum (UHV) PLD system.

a)Authors to whom correspondence should be addressed. Electronic addresses: jiandiz@lsu.edu and wplummer@phys.lsu.edu.

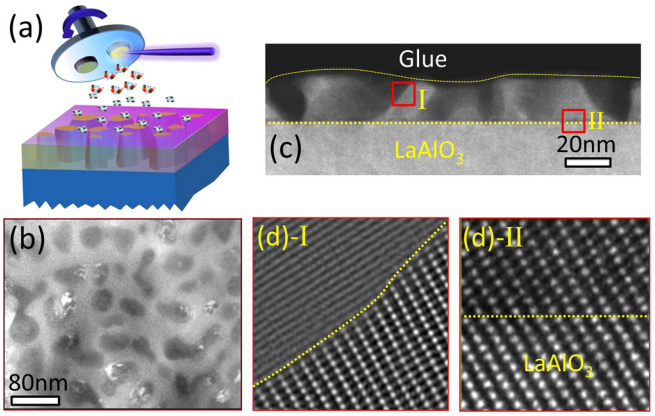

FIG. 1. (a) A schematic view for the growth of nanocomposite with multi-targets in alternate way. TEM images of a $\alpha = 1.3$ nanocomposite LSMO-V_2O_3 thin film on $LaAlO_3$ (111): (b) Planar view in the dark field image and (c) cross-section view of STEM image, showing some columns going through the thin film. (d) High resolution STEM images of the selected regions in (c).

Two stoichiometric LSMO and V_2O_3 sintered targets were installed in a multi-target holder. During deposition, the substrate temperature was maintained at 600 °C under an ozone pressure of 1.3×10^{-7} Torr. A KrF excimer laser ($\lambda = 248$ nm) was used for growing at a repetition rate of 3 Hz. The energy density of the pulsed laser is ~2 J cm^{-2}. The average deposition fluxes for LSMO and V_2O_3 at this condition are 2 Å min^{-1} and 1.3 Å min^{-1}, respectively. To grow LSMO-V_2O_3 nanocomposite, LSMO and V_2O_3 targets were alternately switched *in situ* to the deposition position for certain amount of time for the deposition with LSMO grown first on the substrate. The deposition sequence is expressed as $[(LSMO)_{t_1}(V_2O_3)_{t_2}]_n$, where n is the number of deposition cycles and t_1 and t_2 (min) are the deposition times of LSMO and V_2O_3 in one cycle, respectively. The total deposition time $(t_1 + t_2) \times n$ was about 80 min, which is about 20 nm of thickness, depending on the deposition time ratio of t_2 to t_1. For convenience, the nanocomposite films are labeled with α which is defined as deposition time ratio $\alpha \equiv t_2/t_1$ hereafter.

The structure of thin films was analyzed by diffraction transmission electron microscopy (TEM) (JEOL 3011) and spherical aberration-corrected scanning transmission electron microscopy (STEM) (JOEL 2100F). The chemical composition was extracted by conducting electron-energy-loss-spectroscopy (EELS) mapping via the STEM with sub-Å spatial resolution and ~0.7 eV energy resolution. The transport properties were performed with Quantum Design Physics Properties Measurement System (QD-PPMS) by using 4-probe method and samples with too high resistance were measured with external Keithley 2601 electronics.

Since the lattice of LSMO almost matches LAO, a 2D growth mode was observed for LSMO grown on LAO. For V_2O_3, the large lattice mismatch with LAO substrate results in a 3D island growth. According to our STEM cross-section imaging, the V_2O_3 film in the first ~1.5 nm from the interface shows large lattice distortion with disorder. Only when the film thickness is beyond ~1.5 nm does the film show well-defined crystalline structure. In order to obtain composite film of $[(LSMO)_{t_1}(V_2O_3)_{t_2}]_n$, each deposition time of either LSMO or V_2O_3 cannot be too long. Thick film deposition of individual compound would prevent the complete formation of columnar nanocomposite. In this study, we maintain t_1 and t_2 much less than 80 min and n bigger than 3 for the nanocomposite growth.

Figures 1(b)–1(d) summarize the characterization of the morphology and crystalline structure in the thin film of LSMO-V_2O_3 composite for an intermediate deposition ratio $\alpha = 1.3$ using STEM. Spinodal decomposition type morphology[14] with irregular columnar nanostructure is evident from the planar (Fig. 1(b)) and cross-section (Fig. 1(c)) images. There are dark islands embedded in a bright matrix and separated by ~25 nm in this particular sample. The atomically resolved high angle annular dark field (HAADF) images as displayed in Fig. 1(d) clearly show that these composite structures are crystallized on nanoscale. Thus the alternate deposition of LSMO and V_2O_3 leads to columnar nanocomposites.

The evolution of in-plane morphology and electrical transport properties of the films with different α is presented in Fig. 2. Both $\alpha = 0.4$ and 1.3 samples (see Figs. 2(a) and 2(b)) show similar nanoscale spinodal decomposition type of planar morphology but have different chemical composition as we will discuss later. While $\alpha = 4.33$ sample has a reverse contrast of images and smaller islands as compared to the low α sample. The composite film with $\alpha < 0.8$ exhibits insulating behavior. The sheet resistance as a function of temperature for $\alpha = 0.4$ film is shown in Fig. 2(d) and is very similar to that of a pure 2.4 nm thick LSMO thin film (i.e., $\alpha = 0$) deposited under the same condition on the LAO(111). Note that the LSMO film here has an insulating ground state rather than metallic one exhibited in the bulk crystal. The insulating behavior of 2.4 nm LSMO arises from the dead layer[21] mainly caused by oxygen deficiency[22,23] due to low growth oxygen partial pressure in this study. The higher resistivity in the $\alpha = 0.4$ composite film than that in the pure insulating LSMO film should be related to the disorder and interface strain in the composite film.

In the range of $0.8 \leq \alpha \leq 1.66$ the composite films exhibit metallic behavior ($d\rho/dT > 0$) at high temperature and nonmetallic character ($d\rho/dT < 0$) at low temperature, with the crossover temperature (T_{MIT}) (which is defined as $\frac{dR_s}{dT}|_{T=T_{MIT}} = 0$) depending on the ratio (α). Fig. 2(e) shows the temperature dependent sheet resistance of the films with different α values in this intermediate range, revealing a decrease of T_{MIT} with increasing α. For higher ratio ($\alpha > 1.66$), the electrical resistivity of the composite films is similar to the pure V_2O_3 thin film, because V_2O_3 is dominant in the composite films. As shown in Fig. 2(f), the $\alpha = 4.33$ sample displays a steep increase below ~180 K. Such characteristic is very similar to that of pure 5 nm thick V_2O_3 thin film grown under the same growth condition on LAO(111) and to that of V_2O_3 grown on sapphire.[24]

In the view of that presented in Figs. 2(d)–2(f), we note that R_S for $0.8 \leq \alpha \leq 1.66$ is distinctly different from either low or high α regions with (1) its unique temperature dependence, and (2) 5-7 orders smaller magnitude. This strongly suggests that the composite films in the intermediate regime are qualitatively different from either oxygen-deficient LSMO or V_2O_3. According to the HAADF image, one may suggest that the composite is structured with nanoscale V_2O_3 crystalline pillars (the dark islands in Fig. 2(a)) embedded in

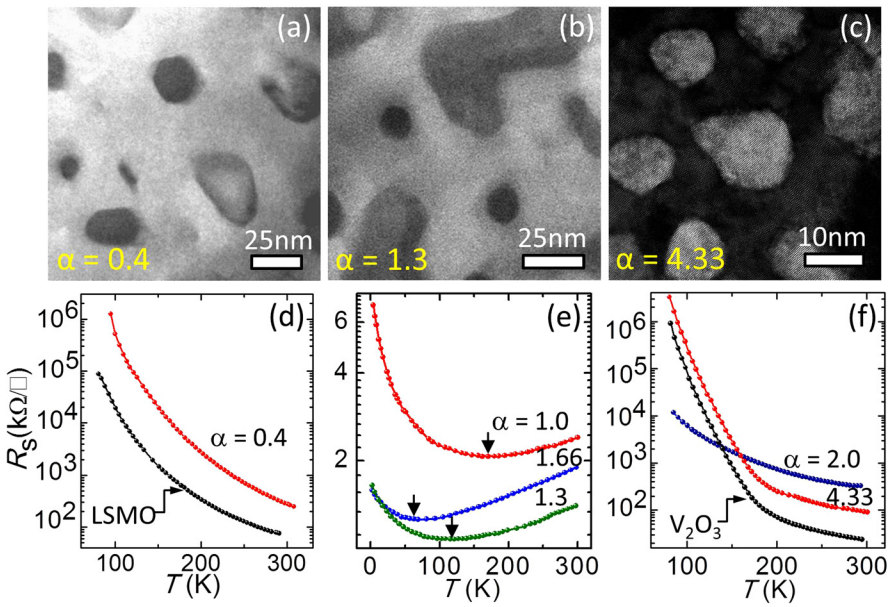

FIG. 2. (a)-(c) Planar view STEM images of different ratio (α) of LSMO-V_2O_3 composite films on $LaAlO_3$ (111); (d)-(f) Temperature (T)-dependence of sheet resistance of the films with (d) $\alpha = 0.4$ (compared with a 2.4 nm LSMO); (e) $\alpha = 1.0$, 1.3, and 1.66; (f) $\alpha = 2.0$ and 4.33 (compared with a 5 nm V_2O_3 film). The arrows indicate the metal-to-nonmetal crossover transition temperature (T_{MIT}).

LSMO matrix in low α region. This is because that the HAADF image is sensitive to atomic number: the heavier the atom is, the brighter the image appears. The nanocomposite films for $\alpha < 0.8$ show strong negative magnetoresistance (MR) effect similar to bulk LSMO, while the a ≥ 0.8 nanocomposite films exhibit almost no or very weak MR effect.[25] For $\alpha > 1.66$, the nanoscale LSMO islands (bright regions) are embedded in the dark V_2O_3 matrix as shown in Fig. 2(c). Apparently, we cannot make similar assignment for the composite films in the intermediate α region, because of their different electrical resistivity behavior.

To determine the chemical composition of the nanoscale composites, we have conducted electron energy loss spectrum (EELS) mapping for different α samples via spherical aberration-corrected STEM. Since the signal of core-loss edges of Sr is too low and noisy for quantitative analysis and oxygen element exists everywhere in the films, we can only focus on the mapping of V, La, and Mn. Fig. 3(a) presents the relative chemical concentration mappings of V, La, and Mn in the marked area of the HAADF image of the $\alpha = 1.3$ composite film. It is clear that the bright region in the area is dominated by La and V with almost no Mn. Surprisingly, Mn is found in the grey region. To further identify the chemical compositions in bright and grey regions, local lattice structures with corresponding lattice constants are characterized using fast Fourier transform (FFT) of high resolution STEM (HRSTEM) cross-section image as shown in Fig. 3(b). The results indicate that the bright region is $La_{1-x}Sr_xVO_3$ (LSVO) and grey one is MnO. Both the EELS mapping and HRSTEM images indicate that LSMO and V_2O_3 react with each other during the deposition, resulting in MnO and LSVO nanocomposite phases in the film.

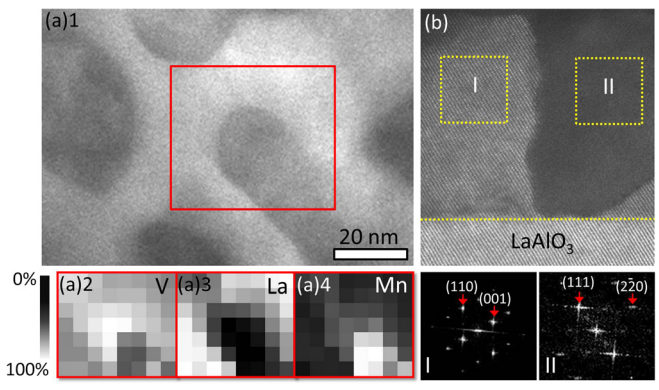

FIG. 3. (a) EELS mapping of $\alpha = 1.3$ LSMO-V_2O_3 composite films on $LaAlO_3$ (111) with STEM: (a)1 Selected mapping area in the planar view in STEM HAADF image and relative concentration of (a)2V-L, (a)3 La-M, and (a)4 Mn-L. (b) High-resolution cross-section image and the FFT images of the selected regions.

The EELS mapping results confirm that LSMO phase is still dominant in the films with $\alpha < 0.8$ although a small amount of LSVO and MnO is also found. Grey MnO pillars are embedded in the dominant LSMO matrix with few nanoscale V_2O_3 pillars. For $\alpha > 1.66$ films, V_2O_3 phase is foremost as appearing in dark regions of Fig. 2(c) with small amount of nanoscale LSVO (bright) and MnO (dark) columns. The structures of the other composite films of $[(LSMO)_{t_1}(V_2O_3)_{t_2}]_n$ with different combination of t_1 and t_2 have been also characterized by STEM and EELS. It is found that, with the same α value but different individual t_1 and t_2, the films exhibit very similar electrical transport properties.[25] It is the deposition ratio α that determines the actual chemical compositions of the grown composite films. The solid state reaction during the growth, which can be tuned by the ratio (α), dictates the geometric structure, chemical phase and physical property in the composite films.

The observed metal-to-nonmetal crossover in the intermediate range ($0.8 \leq \alpha \leq 1.66$) can be explained by a classical percolation scenario. MnO is a good insulator, while the $La_{1-x}Sr_xVO_3$ in bulk crystal has a metal-to-insulator (MIT) transition with transition temperature (T_{MIT}) depending on the doping level.[26] In the case of $x \geq 0.176$, it is metallic at high temperatures but non-metallic below $T_{MIT} \sim 150$ K. For $0.8 \leq \alpha \leq 1.66$, LSVO percolation network is formed in the nanocomposites. Thus, the electrical transport of the nanocomposites is contributed mainly from LSVO network,

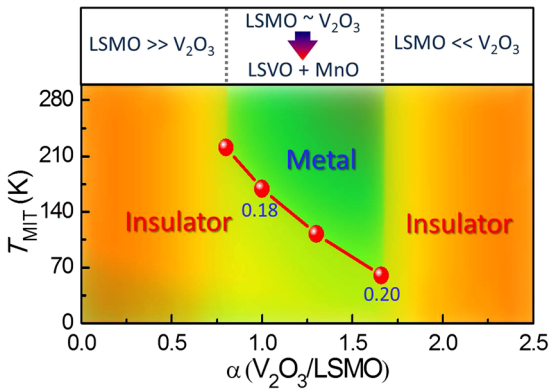

FIG. 4. Phase diagram of LSMO-V_2O_3 nanocomposite films on $LaAlO_3$ (111). The corresponding doping level x of bulk $La_{1-x}Sr_xVO_3$ that has the same T_{MIT} with the nanocomposite is marked. The T_{MIT} of the bulk LSVO is extracted from Ref. 26.

as reflected in the similarly steep increase in electrical resistivity at low temperature. Different α may result in different doping level (x) of LSVO thus exhibiting slightly different T_{MIT}. Furthermore, the out of the plane strain coming from the embedded columnar defects should also affect the properties of LSVO. Both percolation and strain effect determine the T_{MIT} of the nanocomposites. Based upon the electric transport properties of nanocomposites with different α, a phase diagram is constructed as shown in Fig. 4. The advantage here is that, through the alternative deposition technique, one can control the percolative transport by continuously tuning the ratio of different phases.

In summary, we demonstrate that columnar nanocomposite films can be grown by using alternate deposition method. We show that the structure, composition, and physical properties in nanocomposite LSMO-V_2O_3 films on LAO (111) can be turned by a single parameter α—the ratio of deposition times of different compounds. The composition of the resultant nanocomposite film is highly sensitive to the relative amount of deposited LSMO and V_2O_3. In particular, as the amount of LSMO is comparable to V_2O_3, solid state reaction leads to the formation of LSVO and MnO such that the films exhibit a classical percolative transport including the MIT similar to that in the bulk of LSVO. Our results clearly indicate that the structure, chemical composition, and physical properties are determined by the delicate balance between the deposited compounds.

This work was primary supported by U.S. DOE under Grant No. DOE DE-SC0002136.

[1]E. Dagotto, Science **309**, 257 (2005).
[2]A. Ohtomo and H. Y. Hwang, Nature **427**, 423 (2004).
[3]N. Reyren, S. Thiel, A. D. Caviglia, L. F. Kourkoutis, G. Hammerl, C. Richter, C. W. Schneider, T. Kopp, A.-S. Rüetschi, D. Jaccard, M. Gabay, D. A. Muller, J.-M. Triscone, and J. Mannhart, Science **317**, 1196 (2007).
[4]K. Ueda, H. Tabata, and T. Kawai, Science **280**, 1064 (1998).
[5]S. J. May, P. J. Ryan, J. L. Robertson, J.-W. Kim, T. S. Santos, E. Karapetrova, J. L. Zarestky, X. Zhai, S. G. E. te Velthuis, J. N. Eckstein, S. D. Bader, and A. Bhattacharya, Nature Mater. **8**, 892 (2009).
[6]E. Bousquet, M. Dawber, N. Stucki, C. Lichtensteiger, P. Her-met, S. Gariglio, J. M. Triscone, and P. Ghosez, Nature **452**, 732 (2008).
[7]H. Zheng, J. Wang, S. E. Lofland, Z. Ma, L. Mohaddes-Ardabili, T. Zhao, L. Salamanca-Riba, S. R. Shinde, S. B. Ogale, F. Bai, D. Viehland, Y. Jia, D. G. Schlom, M. Wuttig, A. Roytburd, and R. Ramesh, Science **303**, 661 (2004).
[8]S. Kang, A. Goyal, J. Li, A. A. Gapud, P. M. Martin, L. Heatherly, J. R. Thompson, D. K. Christen, F. A. List, M. Paranthaman, and D. F. Lee, Science **311**, 1911 (2006).
[9]J. Cao and J. Wu, Mater. Sci. Eng. R **71**, 35 (2011).
[10]W. Siemons, G. Koster, H. Yamamoto, W. A. Harrison, G. Lucovsky, T. H. Geballe, D. H. A. Blank, and M. R. Beasley, Phys. Rev. Lett. **98**, 196802 (2007).
[11]A. Kalabukhov, R. Gunnarsson, J. Börjesson, E. Olsson, T. Claeson, and D. Winkler, Phys. Rev. B **75**, 121404(R) (2007).
[12]H. Y. Hwang, Y. Iwasa, M. Kawasaki, B. Keimer, N. Nagaosa, and Y. Tokura, Nature Mater. **11**, 103 (2012).
[13]A. V. Boris, Y. Matiks, E. Benckiser, A. Frano, P. Popovich, V. Hinkov, P. Wochner, M. Castro-Colin, E. Detemple, V. K. Malik, C. Bernhard, T. Prokscha, A. Suter, Z. Salman, E. Morenzoni, G. Cristiani, H.-U. Habermeier, and B. Keimer, Science **332**, 937 (2011).
[14]J. L. MacManus-Driscoll, Adv. Funct. Mater. **20**, 2035 (2010).
[15]E. Weal, S. Patnaik, Z. Bi, H. Wang, T. Fix, A. Kursumovic, and J. L. MacManus Driscoll, Appl. Phys. Lett. **97**, 153121 (2010).
[16]H. Yang, H. Y. Wang, J. Yoon, Y. Q. Wang, M. Jain, D. M. Feldmann, Paul C. Dowden, Judith L. Mac-Manus-Driscoll, and Q. X. Jia, Adv. Mater. **21**, 3794 (2009).
[17]J. L. MacManus-Driscoll, P. Zerrer, H. Wang, H. Yang, J. Yoon, S. R. Foltyn, M. G. Blamire, and Q. X. Jia, Nature Mater. **7**, 314 (2008).
[18]O. I. Lebedev, J. Verbeeck, G. Van Tendeloo, O. Shapoval, Belenchuk, V. Moshnyaga, B. Damashcke, and K. Samwer, Phys. Rev. B **66**, 104421 (2002).
[19]A. Urushibara, Y. Moritomo, T. Arima, A. Asamitsu, G. Kido, and Y. Tokura, Phys. Rev. B **51**, 14103 (1995).
[20]D. B. McWhan, A. Menth, J. P. Remeika, W. F. Brinkman, and T. M. Rice, Phys. Rev. B **7**, 1920 (1973).
[21]M. Huijben, L. W. Martin, Y.-H. Chu, M. B. Holcomb, P. Yu, G. Rijnders, D. H. A. Blank, and R. Ramesh, Phys. Rev. B **78**, 094413 (2008).
[22]V. N. Varyukhina, Yu. V. Medvedeva, Yu. M. Nikolaenkoa, A. B. Mukhina, B. V. Belyaevb, V. A. Gritskikhb, I. V. Zhikharevb, S. V. KaraMurzab, N. V. Korchikovab, and A. A. Tikhiib, Tech. Phys. Lett. **35**, 937 (2009).
[23]J.-M. Liu, Q. Huang, J. Li, C. K. Ong, Z. C. Wu, Z. G. Liu, and Y. W. Du, Phys. Rev. B **62**, 8976 (2000).
[24]B. S. Allimi, S. P. Alpay, C. K. Xie, B. O. Wells, J. I. Budnick, and D. M. Pease, Appl. Phys. Lett. **92**, 202105 (2008).
[25]See supplementary material at http://dx.doi.org/10.1063/1.4816596 for the magnetoresistance effect for nanocomposite films and comparison of transport properties between films with same deposition time ratio but different absolute individual deposition time.
[26]S. Miyasaka, T. Okuda, and Y. Tokura, Phys. Rev. Lett. **85**, 5388 (2000).